NANO LETTERS
Cite This: Nano Lett. 2019, 19, 7043−7049
Letter
pubs.acs.org/NanoLett

Valley and Zeeman Splittings in Multilayer Epitaxial Graphene Revealed by Circular Polarization Resolved Magneto-infrared Spectroscopy

Yuxuan Jiang,[†] Zhengguang Lu,[†,‡] Jamey Gigliotti,[§] Avinash Rustagi,[⊥,#] Li Chen,[†] Claire Berger,[§,∥] Walt de Heer,[§,¶] Christopher J. Stanton,[⊥] Dmitry Smirnov,[†] and Zhigang Jiang*[,§]

[†]National High Magnetic Field Laboratory, Tallahassee, Florida 32310, United States
[‡]Department of Physics, Florida State University, Tallahassee, Florida 32306, United States
[§]School of Physics, Georgia Institute of Technology, Atlanta, Georgia 30332, United States
[⊥]Department of Physics, University of Florida, Gainesville, Florida 32611, United States
[∥]Institut Néel, CNRS−Université Grenoble Alpes, 38042 Grenoble, France
[¶]Tianjin International Center of Nanoparticles and Nanosystems, Tianjin University, Tianjin 300072, China

Supporting Information

ABSTRACT: Circular-polarization-resolved magneto-infrared studies of multilayer epitaxial graphene (MEG) are performed using tunable quantum cascade lasers in high magnetic fields up to 17.5 T. Landau level (LL) transitions in the monolayer and bilayer graphene inclusions of MEG are resolved, and considerable electron−hole asymmetry is observed in the extracted electronic band structure. For monolayer graphene, a four-fold splitting of the $n = 0$ to $n = 1$ LL transition is evidenced and attributed to the lifting of the valley and spin degeneracy of the zeroth LL and the broken electron−hole symmetry. The magnetic field dependence of the splitting further reveals its possible mechanisms. The best fit to experimental data yields effective g-factors, $g^*_{VS} = 6.7$ and $g^*_{ZS} = 4.8$, for the valley and Zeeman splittings, respectively.

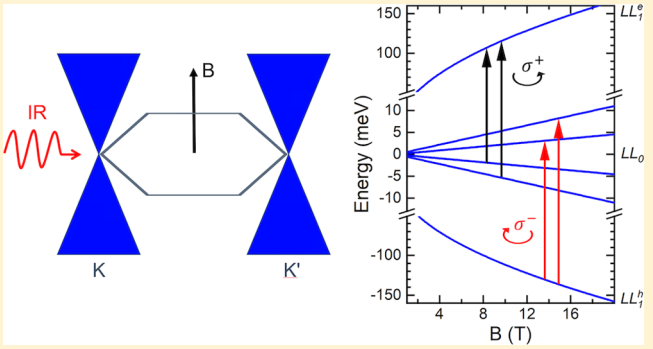

KEYWORDS: *Epitaxial graphene, symmetry breaking states, Landau levels, magneto-infrared spectroscopy*

Graphene has attracted great interest in the past 15 years due to its spectacular physical properties.[1−7] The low-energy electronic structure of graphene features linearly dispersed conduction and valence bands that touch at two inequivalent charge-neutral points (namely K and K' points) in the Brillouin zone.[8] Therefore, electrons in graphene exhibit a four-fold degeneracy, accounting for the spin and K/K' valley symmetry. Broken-symmetry states, particularly at the charge-neutrality point of graphene, have long been a focal point of research.[9−13] To better resolve these states, high-mobility graphene samples and high magnetic fields are typically required, enabling many-particle effects and enhanced spin (Zeeman) and valley splittings in energy. High-field and high-resolution spectroscopy is thus the preferred technique to probe the nature of the broken-symmetry states in graphene.[14−19] This technique provides an accurate measure of the energy splittings as a function of magnetic field (B) for direct comparison with theory.[20]

Epitaxial graphene grown on SiC[21,22] is an ideal platform for implementation of various spectroscopy techniques, owing to its large area, high transparency, and easy means of surface cleaning via high-temperature annealing. The multilayer epitaxial graphene (MEG) grown on the carbon-terminated face of SiC is particularly suited for studying the broken-symmetry states in charge-neutral graphene,[14−16] as the top MEG layers are essentially decoupled from the polar surface of SiC,[23−25] leading to a carrier density as low as 5×10^9 cm^{-2}.[26] The rotational stacking between the top layers also makes them nearly decoupled from each other, rendering an electronic structure indistinguishable from that of an isolated monolayer graphene (MLG).[25,27,28] Record-high mobility of 250 000 cm^2/(V·s) has been reported in top MEG layers, which remains constant at increased temperatures even up to room temperature.[26]

Magneto-infrared (magneto-IR) spectroscopy proves to be a useful tool in probing the broken-symmetry states in charge-neutral graphene.[15,16,29,30] However, the direct evidence to date of the four-fold splitting of the zeroth Landau level (LL)

Received: June 20, 2019
Revised: August 15, 2019
Published: August 30, 2019

DOI: 10.1021/acs.nanolett.9b02505
Nano Lett. 2019, 19, 7043−7049

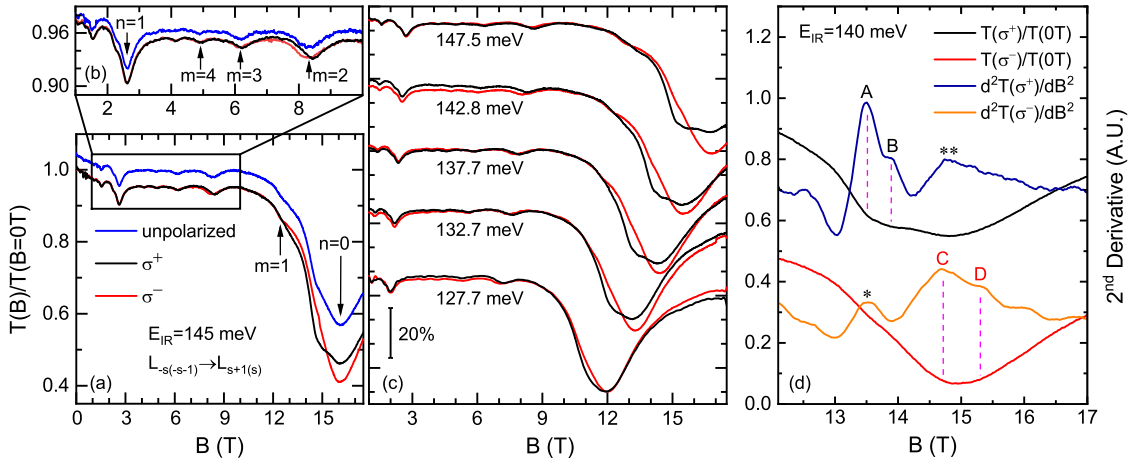

Figure 1. (a) Normalized magneto-transmission spectra, $T(B)/T(B = 0\ \mathrm{T})$, of MEG with σ^+ (black), σ^- (red), and unpolarized (blue) incident IR light at the photon energy $E_{IR} = 145$ meV. The unpolarized spectrum is offset vertically for clarity. The allowed LL transitions in σ^+ (σ^-) polarized light are $LL_{-s} \rightarrow LL_{s+1}$ ($LL_{-s-1} \rightarrow LL_s$), where $s = |n|, |m|$ and integers n and m denote the LL indices of MLG and BLG, respectively. (b) Zoomed-in view of the spectra in (a) between $B = 1$ and 10 T. (c) CP-resolved magneto-transmission spectra measured at different incident photon energies. (d) Comparison of the normalized magneto-transmission spectra with their second derivatives at the incident photon energy $E_{IR} = 140$ meV. The Roman letters label the four-fold splitting of the $n = 0$ LL transition of MLG. The asterisk symbol (*) indicates a weak mode with minor spectral weight, likely due to the CP leakage of our setup, and the double asterisks (**) label a broad mode that carries considerable spectral weight and with a transition energy corresponding to $v_F = 1.00 \times 10^6$ m/s. In (c,d), the spectra are also offset vertically for clarity.

only comes from the electronic transport and tunneling spectroscopy measurements, where the energy splittings are enhanced when the Fermi energy is placed within the gap between two split sub-LLs. The interpretation of the electronic transport measurements in Hall-bar-like device geometries is also complicated by the (extrinsic) conditions of the graphene edge,[31,32] which may be of a different nature from that in the bulk.[33] In this work, via combining the bulk-sensitive circular-polarization (CP)-resolved magneto-IR spectroscopy with high-quality quasi-neutral MEGs, we are able to probe the valley and Zeeman splittings (VS and ZS) of graphene LLs in high magnetic fields. CP-resolved measurements are known to be sensitive in revealing fine LL structures due to its selective activation of the electron-like or hole-like transitions.[34−36] Therefore, it can yield important information on the electron−hole asymmetry of the material's band structure. The long lifetime of Dirac fermions in MEG and the application of high magnetic fields also enable the high-energy resolution of our measurements and distinguish our work from previous CP-resolved studies of graphene.[37,38] Our magnetic-field-dependent measurements lead to the determination of effective g-factors for ZS and VS, which are key to understanding the rich phase diagram of charge-neutral graphene in high magnetic fields[39] and its implications in MEG.

MEG samples were grown on the carbon-terminated face of SiC using the confinement-controlled sublimation method,[21,22] followed by routine atomic force microscopy (Park System XE) and Raman spectroscopy characterizations. The high-quality samples (~30 layers) were selected based on the surface morphology and the absence of the D peak in the Raman spectra[40] and loaded in a home-built free-space magneto-IR dipper equipped with a superconducting magnet. The IR transmission measurements were performed at 4.2 K in a Faraday configuration with both circularly polarized and unpolarized light emitted from a set of quantum cascade lasers covering the spectral range between 100 and 200 meV. However, due to the overlap with the SiC reststrahlen band, no transmission signal was detected below 124 meV. For CP-resolved measurements, the polarized light was generated by placing a linear polarizer and a wavelength-tunable quarter waveplate in the optical path. For consistency, the CP-resolved spectra were taken by fixing the light polarization and sweeping the magnetic field in positive or negative directions, which is equivalent to the use of σ^+ and σ^- polarized light. The details of the experimental setup can be found in the Supporting Information as well as in our previous work.[41]

Figure 1a,b shows the typical magneto-transmission spectra of MEG, $T(B)/T(B = 0\ \mathrm{T})$, measured with incident IR light at the photon energy $E_{IR} = 145$ meV and normalized to its zero-field value. From the unpolarized (blue) spectra, one can identify a series of absorption dips or modes, and following previous work,[42] one can attribute them to two distinct sequences of inter-LL transitions, with the dominant sequence originated from MLG and the second sequence from AB-stacked bilayer graphene (BLG). The presence of a small amount of AB-stacked BLG inclusions in MEG is well understood from previous spectroscopy studies.[42−45] Notably, this presence is due to the stacking faults (AB-stack) in the otherwise rotationally stacked (~30° with respect to each other) and electronically decoupled top MEG layers. Therefore, all of the absorption modes observed in our experiment can be described with the LL spectra of MLG and BLG:[46,47]

$$E_{\mathrm{MLG},n} = \mathrm{sgn}(n)\sqrt{2e\hbar v_F^2|n|B} \tag{1}$$

$$E_{\mathrm{BLG},m} = \frac{\mathrm{sgn}(m)}{\sqrt{2}} \times \left[(2|m| + 1)\Delta_B^2 + \gamma_1^2 - \sqrt{\gamma_1^4 + 2(2|m| + 1)\Delta_B^2\gamma_1^2 + \Delta_B^4}\right]^{1/2} \tag{2}$$

where e is the elementary electron charge, $\hbar$ is the reduced Planck's constant, v_F is the Fermi velocity, integer n (m) is the LL index of MLG (BLG), and $n > 0$ ($m > 0$) or $n < 0$ ($m < 0$) represents electron or hole LLs. The Fermi velocity v_F is also related to the intralayer hopping parameter γ_0 and determines the cyclotron energy of MLG through $\Delta_B \equiv v_F\sqrt{2e\hbar B}$. γ_1 is an

DOI: 10.1021/acs.nanolett.9b02505
Nano Lett. 2019, 19, 7043−7049

interlayer coupling parameter of BLG, describing the relatively strong coupling between two carbon atoms stacked directly on top of each other. The corresponding LL transitions are expected to be $LL_{-s(-s-1)} \rightarrow LL_{s+1(s)}$ (which are referred to as the s transition throughout this work), following the usual selection rule $\Delta s = \pm 1$ with integer $s = |n|, |m|$.

Using σ^+ and σ^- polarized light, one can perform the CP-resolved measurements and probe the electron-like ($LL_{-s} \rightarrow LL_{s+1}$, $\Delta s = +1$, σ^+ active) and hole-like ($LL_{-s-1} \rightarrow LL_s$, $\Delta s = -1$, σ^- active) transitions separately. Figure 1a–c shows the CP-resolved magneto-transmission spectra of MEG measured at selected incident photon energies. A prominent difference in spectral line shape between the $LL_{n=0} \rightarrow LL_{n=1}$ (black) and $LL_{n=-1} \rightarrow LL_{n=0}$ (red) transitions is clearly evidenced, and it becomes more pronounced with increasing photon energy. This observation is suggestive of considerable electron–hole asymmetry in the electronic structure of top MEG layers, which, in the literature,[48] has simply been described by assigning a larger Fermi velocity for the electrons than the holes, $v_F^e > v_F^h$.

It is worth noting that asymmetry in magneto-transmission spectra has previously been reported in the CP-resolved measurements of a *thin* MEG sample (~5 layers),[37] where a low-energy mode is observed only with σ^+ polarized light and attributed to the $LL_{n=0} \rightarrow LL_{n=1}$ transition in the doped layers close to the graphene/SiC interface. The doped graphene layers near the interface are known to have low electron mobility and thus exhibit a smaller Fermi velocity and lower LL transition energies for a given magnetic field.[49,50] In our case, however, the additional σ^+-active modes occur at a lower magnetic field (Figure 1a,c). That is, they occur at higher energies if measured in a constant magnetic field, as compared to the σ^--active modes. This behavior is in sharp contrast to previous work.[37] In addition, our MEG sample is much thicker, similar to that studied in ref 26 with record-high mobility.

Further careful inspection and second derivative calculation of the measured magneto-transmission spectra of MEG reveal fine structures or modes within the $n = 0$ LL transition, as shown in Figure 1d. Four distinct modes, labeled by Roman letters A, B, C, and D, can be readily identified via correlating a kink feature in the spectra with a peak in its second derivative, especially at high incident photon energies. The additional peak, labeled by the asterisk symbol (*) in the second derivative, indicates a weak σ^--active mode with minor spectral weight, likely due to the CP leakage of our experiment setup. The double asterisks (**), on the other hand, label a broad σ^+-active mode that carries considerable spectral weight and with a transition energy corresponding to $v_F = 1.00 \times 10^6$ m/s. As in high-mobility MLG, the many-particle effects tend to renormalize the bands, giving rise to a larger Fermi velocity near the charge neutrality,[46,52] and cause ZS and VS of the zeroth LL, one can attribute the A, B, C, and D modes to the four-fold splitting of the $n = 0$ transition in high-mobility graphene layers but attribute the ** mode to the layers with relatively low mobility (see Supporting Information for further discussion of the MEG structure).

Figure 2a shows the Landau fan diagram of MLG near charge neutrality, considering the four-fold splitting of the zeroth LL and the electron–hole asymmetry. For simplicity, we schematically neglect the splittings of the first electron and hole LLs, E_1^e and E_1^h, which can simply be added back in at the end of our analysis. The modes labeled by A, B, C, and D in Figure 1d can then be assigned to T_A, T_B, T_C, and T_D transitions in Figure 2a, given that T_A and T_B are electron-like and $T_A > T_B$ while T_C and T_D are hole-like and $T_C > T_D$. These transitions can be quantitatively described using the following LL or sub-LL energies:

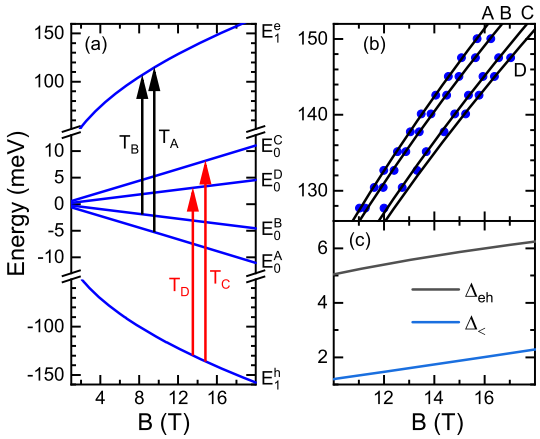

Figure 2. (a) Landau fan diagram of MLG near charge neutrality. The four-fold splitting of the $n = 0$ transition is labeled by T_A, T_B, T_C, and T_D, corresponding to the modes A, B, C, and D in Figure 1d, respectively. As the top MEG layers are quasi-neutral, none of these transitions are expected to be Pauli-blocked. (b) Evolution of the modes A, B, C, and D (blue dots) in the energy–magnetic-field space. The solid lines are best fit to the data using eq 5. (c) Magnetic field dependence of $\Delta_<$ and Δ_{eh} calculated from eq 4.

$$E_1^e = v_F^e\sqrt{2e\hbar B}, \quad E_1^h = -v_F^h\sqrt{2e\hbar B}$$
$$E_0^C = -E_0^A = \frac{\Delta_>(B) + \Delta_<(B)}{2}$$
$$E_0^D = -E_0^B = \frac{\Delta_>(B) - \Delta_<(B)}{2} \quad (3)$$

where the electron–hole asymmetry is reflected in E_1^e and E_1^h, and as there is no consensus on the relative magnitude of the ZS and VS, $\Delta_>$ and $\Delta_<$ are employed to denote the larger and smaller splitting between the two, respectively. Both $\Delta_>$ and $\Delta_<$ are expected to have a distinct magnetic field dependence, depending on its underlying mechanism to be discussed below.

From eq 3, one can deduce the values of $\Delta_<$ and $\Delta_{eh} \equiv E_1^e + E_1^h$ (which describes the degree of electron–hole asymmetry at a given magnetic field) using experimental parameters $T_{A,B,C,D}$:

$$\Delta_< = \frac{(T_A - T_B) + (T_C - T_D)}{2}$$
$$\Delta_{eh} = \frac{(T_A + T_B) - (T_C + T_D)}{2} \quad (4)$$

Practically, this is done by taking the CP-resolved measurements at various incident photon energies and extracting the corresponding magnetic fields of $T_{A,B,C,D}$ transitions. The results are then plotted in the energy–magnetic-field space (as shown in Figure 2b), where the energy of each mode can be interpolated for any given magnetic field. For best interpolation, one can fit the magnetic field dependence of each mode with

$$T_i = a_i\sqrt{B} + b_iB, \quad i = \text{A, B, C, D} \quad (5)$$

DOI: 10.1021/acs.nanolett.9b02505
Nano Lett. 2019, 19, 7043–7049

as the VS and ZS of the zeroth LL in MLG are expected to be either $\propto\sqrt{B}$ or $\propto B$.[39] In eq 5, a_i and b_i are the fitting parameters for mode i.

Figure 2c shows the deduced $\Delta_<$ and Δ_{eh} as a function of magnetic field. Although the effective magnetic field range of the measurements (for the n = 0 LL transition) is limited to between 11 and 17 T, one can still ascertain a linear-in-B dependence of $\Delta_<$ with $\Delta_<$ = 0 meV at zero magnetic field. Such a linear dependence helps identify $\Delta_<$ as Zeeman-like splitting with an enhanced g-factor while leaving $\Delta_>$ as a result of broken valley degeneracy of the zeroth LL. This assignment excludes the spin-polarized ferromagnetic state as the ground state of charge-neutral graphene, in accordance with prior studies.[12,13,15,16,19]

In addition, as a consistency check, the magnetic field dependence of Δ_{eh} (Figure 2c) is examined and found to be $\propto\sqrt{B}$, considering Δ_{eh} = 0 meV as $B \to 0$. This observation is consistent with that expected from eq 3, validating the interpolation procedure undertaken. The magnitude of Δ_{eh}, however, is several times larger than $\Delta_<$ and comparable with $\Delta_>$ (to be discussed next). Therefore, electron−hole asymmetry is an important factor in determining the splitting energies.

Except for the spin-polarized ferromagnetic state, there are three other possible symmetry-breaking states theoretically predicted for $\Delta_>$ of MLG,[39] namely, the canted antiferromagnetic, charge density wave, and Kekulé distortion states. Although the previous electronic transport study[13] of MLG encapsulated in h-BN is in favor of the canted antiferromagnetic state (where the edge states dominate charge transport), bulk-sensitive spectroscopy studies of MEG lead to the charge density wave[15,16] and Kekulé distortion[19] state interpretations, leaving the nature of $\Delta_>$ still an open question. Unfortunately, because the determination of $\Delta_>$ requires additional information about the Fermi velocity than just the experimental parameters $T_{A,B,C,D}$ and our model describing the electron−hole asymmetry is oversimplified, this work cannot give a conclusive answer to this question. Instead, we carry out a validity check on the two possible scenarios, (i) $\Delta_> \propto \sqrt{B}$[20] and (ii) $\Delta_> \propto B$,[51] and provides a set of parameters that can best explain the experimental data.

To determine $\Delta_>$, one can fit all the LL transitions (MLG) observed, including the four-fold splitting of the n = 0 transition, the n = 1 and n = 2 transitions with eqs 1 and 3. The black solid lines in Figure 3 show the best fit to the data with most of the weight on the n = 0 transition. For case (i), the corresponding fitting parameters are $v_F^e = 1.025 \times 10^6$ m/s, $v_F^h = 0.975 \times 10^6$ m/s, $\Delta_< = 0.16$ meV/T, $\Delta_> = 1.44$ meV/$\sqrt{T}$, and the coefficient of determination for the fitting to the n = 0 transition is as high as R^2 = 0.98. The slight deviation between the fits to the n = 1 and n = 2 transitions and the experimental data can be attributed to the contribution from electron−electron interactions, as described previously.[20,46,49,50] The fit for case (ii) only results in small differences in the n = 0 transition, as indicated by the red dashed lines in Figure 3 with $\Delta_>$ = 0.39 meV/T. Although within the experimental uncertainty, one cannot differentiate the above two cases, it is still insightful to have a closer look at the fitting parameters. First, the extracted Fermi velocities and the electron−hole asymmetry (±2.5%) are consistent with those reported in previous works.[24,26,27,48,52] Second, $\Delta_<$ = 0.16 meV/T is corresponding to a ZS with a g-factor of 2.8. After considering the additional contribution from the ZS of the first LL with a bare electron g-factor of 2,[9] the total effective g-factor reaches g^*_{ZS} = 4.8. Third, $\Delta_>$ = 1.44 meV/$\sqrt{T}$ of case (i) can be attributed to an electron−electron interaction induced VS. However, the induced energy gap is estimated to be on the order of Coulomb energy,[20] $e^2/4\pi\epsilon\epsilon_0 l_B \approx 11$ meV/$\sqrt{T}$, much larger than the experimental value. Here, $l_B = \sqrt{\hbar/eB}$ is the magnetic length and $\epsilon \approx 5$ and ϵ_0 are the relative permittivity of MEG and the vacuum permittivity, respectively.[53] Lastly, $\Delta_>$ = 0.39 meV/T of case (ii) can either originate from the charge density wave[15,16] or the Kekulé distortion[19] state as a result of the electron−phonon interaction. Such interaction lowers the ground state energy by slightly distorting the graphene lattice in a way that breaks the inversion symmetry and leads to VS.[51] The resulting energy contribution is proportional to the electron degeneracy of each sub-LL, therefore exhibiting a linear-in-B dependence. This case seems to best explain our experimental findings, with an effective VS g-factor of g^*_{VS} = 6.7.

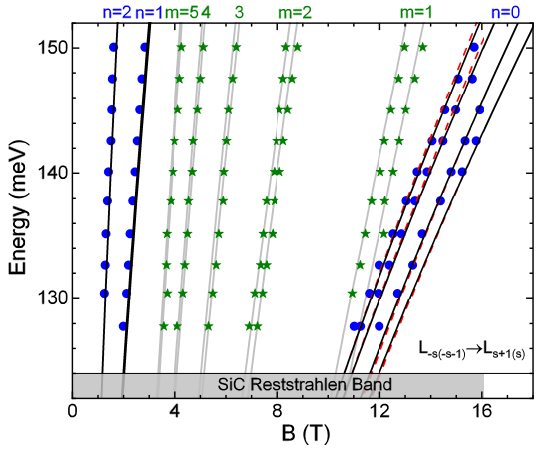

Figure 3. Magnetic field dependence of the observed LL transitions from the MLG (blue dots) and BLG (green stars) inclusions in MEG. The black solid (red dash) lines are the best fit to the MLG transitions using eqs 1 and 3 and assuming $\Delta_> \propto \sqrt{B}$ ($\Delta_> \propto B$), whereas the gray lines are the best fit to the BLG transitions. The darker gray area represents the experimentally inaccessible spectral region due to the SiC reststrahlen band.

Before closing, we would like to discuss another interesting behavior revealed by the CP-resolved spectra of the BLG inclusions in MEG, that is, pronounced electron−hole asymmetry but with the opposite sign to that in MLG. Figure 4a shows the normalized magneto-transmission spectra of the m = 2 LL transition of BLG measured with σ^+ (black) and σ^- (red) polarized light at different incident photon energies. Here, the σ^--active transitions (dips) always appear on the low field side of the σ^+-active transitions, in sharp contrast to the n = 0 transition of MLG in Figure 1c. Such behavior occurs in all BLG transitions observed, especially the m = 1 and m = 2 transitions, as also implied in Figure 3.

To quantitatively understand this behavior, one can fit the BLG transitions (green stars in Figure 3) with eq 2. Due to the massive Dirac fermion nature of the electrons and holes in BLG, the fitting can be performed by fixing the Fermi velocity to its MLG value, $v_F = 1.02 \times 10^6$ m/s, measured with unpolarized light,[42] whereas differentiating the band mass of electrons and holes via $m^*_{e,h} = \gamma_1^{e,h}/2v_F^2$. The gray lines in Figure 3 show the best fit to the five BLG transitions observed in the experiment, and the corresponding fitting parameters are m^*_e = $0.0376m_0$ and m^*_h = $0.0283m_0$, where m_0 is the bare electron

DOI: 10.1021/acs.nanolett.9b02505
Nano Lett. 2019, 19, 7043−7049

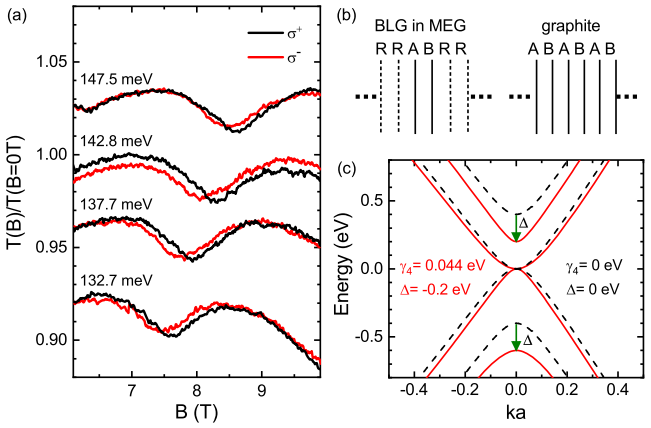

Figure 4. (a) Normalized magneto-transmission spectra of the $m = 2$ LL transition of BLG measured with σ^+ (black) and σ^- (red) polarized light at different incident photon energies. (b) Schematics of the rotational stacking order between graphene layers in MEG and AB-stacked graphite. The letters A, B, and R denote three different rotation angles of a graphene plane, which are 0, 60, and 30°, respectively. (c) Low-energy band structure of BLG with (red) and without (black) electron−hole asymmetry. For both cases, the bands are plotted using $\gamma_0 = 3.16$ eV and $\gamma_1 = 0.4$ eV. k is the wave vector, and $a = 2.46$ Å is the lattice constant of graphene. The electron−hole asymmetry is introduced by assigning $\gamma_4 = 0.044$ eV and $\Delta = -0.2$ eV. For demonstration purposes, Δ is taken to be about 3 times larger than the extracted value (−0.068 eV) from experiment.

mass. The coefficient of determination of the BLG fitting is $R^2 = 0.97$. The magnitude of the electron−hole asymmetry is then ±14%, consistent with that extracted from the splittings of the $m = 1$ and $m = 2$ transitions in the previous magneto-IR study of MEG.[42]

The sign of the electron−hole asymmetry in the BLG inclusions, however, is in stark contrast to the existing literature on exfoliated BLG,[47,54−57] where a lighter electron mass is always expected. Such an anomaly ought to be associated with the multilayer nature of MEG, particularly the coupling between the BLG and its neighboring layers. To examine this possibility, one can take an extreme case and compare the tight-binding parameters of BLG with AB-stacked graphite.[58] The presence of additional graphene layers in graphite is found to strongly influence the skew interlayer coupling parameter γ_4 and the energy difference Δ between the dimer and nondimer sites. As γ_4 and Δ are the two primary sources for the electron−hole asymmetry in BLG and the value of Δ can be either positive or negative,[58,59] it is not surprising to see a different sign for the electron−hole asymmetry in MEG due to its unique stacking order (Figure 4b) and coupling between layers. Figure 4c shows a possible electronic band structure of BLG that can explain our experimental data. Here, instead of using the phenomenological band mass $m^*_{e,h}$, the electron−hole asymmetry is introduced by γ_4 and Δ, while setting $\gamma_0 = 3.16$ eV (corresponding to $v_F = 1.02 \times 10^6$ m/s) and $\gamma_1 = 0.4$ eV. $m^*_e > m^*_h$ observed in the experiment corresponds to $\Delta < 0$, which could be due to the local potential changes caused by the rotational stacked graphene layers (with different rotation angles) above and below the BLG and the next-nearest layer couplings.[58,59] Quantitatively, the amount of electron−hole asymmetry can be expressed as $\pm\left(\frac{\Delta}{\gamma_1} + \frac{2\gamma_4}{\gamma_0}\right) = \pm 14\%$.[42,58] By fixing $\gamma_4 = 0.044$ eV, as that in graphite, one can obtain $\Delta = -0.068$ eV for MEG.

In conclusion, we have performed a magneto-IR spectroscopy study of high-quality MEG with tunable CP light. We find that the MLG inclusions in MEG feature a four-fold splitting of the $n = 0$ LL transition, resulting from the lifting of the valley and spin degeneracy of the zeroth LL and the broken electron−hole symmetry. By analyzing the magnetic field dependence of the transition energies, we deduce a possible scenario that involves VS at the charge neutrality and enhanced ZS in the electron and hole sub-LLs. The extracted effective g-factors are $g^*_{VS} = 6.7$ and $g^*_{ZS} = 4.8$. The CP-resolved measurements of the BLG inclusions uncover an even larger electron−hole asymmetry, with an opposite sign to the MLG. We show that the asymmetry could be strongly influenced by the stacking orientation of the BLG (with respect to the neighboring layers), making it a possible design parameter for future epitaxial graphene band engineering.

■ ASSOCIATED CONTENT

Supporting Information

The Supporting Information is available free of charge on the ACS Publications website at DOI: 10.1021/acs.nanolett.9b02505.

Details of the experiment setup and MEG characterization (PDF)

■ AUTHOR INFORMATION

Corresponding Author

*E-mail: zhigang.jiang@physics.gatech.edu.

ORCID

Dmitry Smirnov: 0000-0001-6358-3221

Zhigang Jiang: 0000-0001-9884-3337

Present Address

#School of Electrical and Computer Engineering, Purdue University, West Lafayette, Indiana 47907, USA.

Notes

The authors declare no competing financial interest.

■ ACKNOWLEDGMENTS

We thank Edward Conrad, Phillip First, Markus Kindermann, and Kun Yang for helpful discussions. This work was primarily supported by the DOE (Grant No. DE-FG02-07ER46451). The MEG growth and characterization at GT were supported by the NSF (Grant No. DMR-0820382) and the NASA Solar System Exploration Research Virtual Institute (cooperative agreement NNA17BF68A). The magneto-IR measurements were performed at the NHMFL, which is supported by the NSF through cooperative agreement DMR-1157490/1644779 and the State of Florida. A.R. and C.J.S. were supported by the Air Force Office of Scientific Research under Award Nos. FA9550-14-1-0376 and FA9550-17-1-0341. L.C. was supported in part by the DOE, Office of BES, through Grant No. DE-SC0002140. C.B. acknowledges partial funding from the EU flagship graphene (Grant No. 604391). Z.J. acknowledges support from the NHMFL Visiting Scientist Program.

■ REFERENCES

(1) Beenakker, C. W. J. Colloquium: Andreev Reflection and Klein Tunneling in Graphene. *Rev. Mod. Phys.* **2008**, *80*, 1337−1354.

(2) Castro Neto, A. H.; Guinea, F.; Peres, N. M. R.; Novoselov, K. S.; Geim, A. K. The Electronic Properties of Graphene. *Rev. Mod. Phys.* **2009**, *81*, 109−162.

DOI: 10.1021/acs.nanolett.9b02505
Nano Lett. 2019, 19, 7043−7049

(3) Peres, N. M. R. Colloquium: The Transport Properties of Graphene: An Introduction. *Rev. Mod. Phys.* **2010**, *82*, 2673−2700.
(4) Das Sarma, S.; Adam, S.; Hwang, E. H.; Rossi, E. Electronic Transport in Two-Dimensional Graphene. *Rev. Mod. Phys.* **2011**, *83*, 407−470.
(5) Goerbig, M. O. Electronic Properties of Graphene in a Strong Magnetic Field. *Rev. Mod. Phys.* **2011**, *83*, 1193−1243.
(6) Kotov, V. N.; Uchoa, B.; Pereira, V. M.; Guinea, F.; Castro Neto, A. H. Electron-Electron Interactions in Graphene: Current Status and Perspectives. *Rev. Mod. Phys.* **2012**, *84*, 1067−1125.
(7) Basov, D. N.; Fogler, M. M.; Lanzara, A.; Wang, F.; Zhang, Y. Colloquium: Graphene Spectroscopy. *Rev. Mod. Phys.* **2014**, *86*, 959−994.
(8) Wallace, P. R. The Band Theory of Graphite. *Phys. Rev.* **1947**, *71*, 622−634.
(9) Zhang, Y.; Jiang, Z.; Small, J. P.; Purewal, M. S.; Tan, Y.-W.; Fazlollahi, M.; Chudow, J. D.; Jaszczak, J. A.; Stormer, H. L.; Kim, P. Landau-Level Splitting in Graphene in High Magnetic Fields. *Phys. Rev. Lett.* **2006**, *96*, 136806.
(10) Jiang, Z.; Zhang, Y.; Stormer, H. L.; Kim, P. Quantum Hall States near the Charge-Neutral Dirac Point in Graphene. *Phys. Rev. Lett.* **2007**, *99*, 106802.
(11) Zhao, Y.; Cadden-Zimansky, P.; Ghahari, F.; Kim, P. Magnetoresistance Measurements of Graphene at the Charge Neutrality Point. *Phys. Rev. Lett.* **2012**, *108*, 106804.
(12) Young, A. F.; Dean, C. R.; Wang, L.; Ren, H.; Cadden-Zimansky, P.; Watanabe, K.; Taniguchi, T.; Hone, J.; Shepard, K. L.; Kim, P. Spin and Valley Quantum Hall Ferromagnetism in Graphene. *Nat. Phys.* **2012**, *8*, 550−556.
(13) Young, A. F.; Sanchez-Yamagishi, J. D.; Hunt, B.; Choi, S. H.; Watanabe, K.; Taniguchi, T.; Ashoori, R. C.; Jarillo-Herrero, P. Tunable Symmetry Breaking and Helical Edge Transport in a Graphene Quantum Spin Hall State. *Nature* **2014**, *505*, 528−532.
(14) Song, Y. J.; Otte, A. F.; Kuk, Y.; Hu, Y.; Torrance, D. B.; First, P. N.; de Heer, W. A.; Min, H.; Adam, S.; Stiles, M. D.; et al. High-Resolution Tunnelling Spectroscopy of a Graphene Quartet. *Nature* **2010**, *467*, 185−189.
(15) Orlita, M.; Tan, L. Z.; Potemski, M.; Sprinkle, M.; Berger, C.; de Heer, W. A.; Louie, S. G.; Martinez, G. Resonant Excitation of Graphene K-Phonon and Intra-Landau-Level Excitons in Magneto-Optical Spectroscopy. *Phys. Rev. Lett.* **2012**, *108*, 247401.
(16) Tan, L. Z.; Orlita, M.; Potemski, M.; Palmer, J.; Berger, C.; de Heer, W. A.; Louie, S. G.; Martinez, G. SU(4) Symmetry Breaking Revealed by Magneto-Optical Spectroscopy in Epitaxial Graphene. *Phys. Rev. B: Condens. Matter Mater. Phys.* **2015**, *91*, 235122.
(17) Hunt, B. M.; Li, J.; Zibrov, A. A.; Wang, L.; Taniguchi, T.; Watanabe, K.; Hone, J.; Dean, C. R.; Zaletel, M.; Ashoori, R. C.; Young, A. F. Direct Measurement of Discrete Valley and Orbital Quantum Numbers in Bilayer Graphene. *Nat. Commun.* **2017**, *8*, 948.
(18) Li, S.-Y.; Ren, Y.-N.; Liu, Y.-W.; Chen, M.-X.; Jiang, H.; He, L. Nanoscale Detection of Valley-Dependent Spin Splitting around Atomic Defects of Graphene. *2D Mater.* **2019**, *6*, 031005.
(19) Li, S.-Y.; Zhang, Y.; Yin, L.-J.; He, L. Scanning Tunneling Microscope Study of Quantum Hall Isospin Ferromagnetic States of Zero Landau Level in Graphene Monolayer. *Phys. Rev. B: Condens. Matter Mater. Phys.* **2019**, *100*, 085437.
(20) For example, see an earlier review: Yang, K. Spontaneous Symmetry Breaking and Quantum Hall Effect in Graphene. *Solid State Commun.* **2007**, *143*, 27−32 and the references therein .
(21) de Heer, W. A.; Berger, C.; Ruan, M.; Sprinkle, M.; Li, X.; Hu, Y.; Zhang, B.; Hankinson, J.; Conrad, E. Large Area and Structured Epitaxial Graphene Produced by Confinement Controlled Sublimation of Silicon Carbide. *Proc. Natl. Acad. Sci. U. S. A.* **2011**, *108*, 16900−16905.
(22) Berger, C.; Conrad, E. H.; de Heer, W. A. Epigraphene: Epitaxial Graphene on Silicon Carbide. In *Landolt-Börnstein: Numerical Data and Functional Relationships in Science and Technology - New Series*, Physics of Solid Surfaces, Subvolume B-VIII; Chiarotti, G., Chiaradia, P., Eds.; Springer-Verlag: Berlin, 2018; Vol. *45*, pp 665−748.
(23) Varchon, F.; Feng, R.; Hass, J.; Li, X.; Ngoc Nguyen, B.; Naud, C.; Mallet, P.; Veuillen, J.-Y.; Berger, C.; Conrad, E. H.; Magaud, L. Electronic Structure of Epitaxial Graphene Layers on SiC: Effect of the Substrate. *Phys. Rev. Lett.* **2007**, *99*, 126805.
(24) Miller, D. L.; Kubista, K. D.; Rutter, G. M.; Ruan, M.; de Heer, W. A.; First, P. N.; Stroscio, J. A. Observing the Quantization of Zero Mass Carriers in Graphene. *Science* **2009**, *324*, 924−927.
(25) Sprinkle, M.; Siegel, D.; Hu, Y.; Hicks, J.; Tejeda, A.; Taleb-Ibrahimi, A.; Le Fèvre, P.; Bertran, F.; Vizzini, S.; Enriquez, H.; et al. First Direct Observation of a Nearly Ideal Graphene Band Structure. *Phys. Rev. Lett.* **2009**, *103*, 226803.
(26) Orlita, M.; Faugeras, C.; Plochocka, P.; Neugebauer, P.; Martinez, G.; Maude, D. K.; Barra, A.-L.; Sprinkle, M.; Berger, C.; de Heer, W. A.; Potemski, M. Approaching the Dirac Point in High-Mobility Multilayer Epitaxial Graphene. *Phys. Rev. Lett.* **2008**, *101*, 267601.
(27) Sadowski, M. L.; Martinez, G.; Potemski, M.; Berger, C.; de Heer, W. A. Landau Level Spectroscopy of Ultrathin Graphite Layers. *Phys. Rev. Lett.* **2006**, *97*, 266405.
(28) Hass, J.; Varchon, F.; Millán-Otoya, J. E.; Sprinkle, M.; Sharma, N.; de Heer, W. A.; Berger, C.; First, P. N.; Magaud, L.; Conrad, E. H. Why Multilayer Graphene on 4H-SiC($000\bar{1}$) Behaves Like a Single Sheet of Graphene. *Phys. Rev. Lett.* **2008**, *100*, 125504.
(29) Henriksen, E. A.; Cadden-Zimansky, P.; Jiang, Z.; Li, Z. Q.; Tung, L.-C.; Schwartz, M. E.; Takita, M.; Wang, Y.-J.; Kim, P.; Stormer, H. L. Interaction-Induced Shift of the Cyclotron Resonance of Graphene Using Infrared Spectroscopy. *Phys. Rev. Lett.* **2010**, *104*, 067404.
(30) Chen, Z.-G.; Shi, Z.; Yang, W.; Lu, X.; Lai, Y.; Yan, H.; Wang, F.; Zhang, G.; Li, Z. Q. Observation of an Intrinsic Bandgap and Landau Level Renormalization in Graphene/Boron-Nitride Heterostructures. *Nat. Commun.* **2014**, *5*, 4461.
(31) Cui, Y.-T.; Wen, B.; Ma, E. Y.; Diankov, G.; Han, Z.; Amet, F.; Taniguchi, T.; Watanabe, K.; Goldhaber-Gordon, D.; Dean, C. R.; Shen, Z.-X. Unconventional Correlation between Quantum Hall Transport Quantization and Bulk State Filling in Gated Graphene Devices. *Phys. Rev. Lett.* **2016**, *117*, 186601.
(32) Zhu, M. J.; Kretinin, A. V.; Thompson, M. D.; Bandurin, D. A.; Hu, S.; Yu, G. L.; Birkbeck, J.; Mishchenko, A.; Vera-Marun, I. J.; Watanabe, K.; et al. Edge Currents Shunt the Insulating Bulk in Gapped Graphene. *Nat. Commun.* **2017**, *8*, 14552.
(33) Zeng, Y.; Li, J. I. A.; Dietrich, S. A.; Ghosh, O. M.; Watanabe, K.; Taniguchi, T.; Hone, J.; Dean, C. R. High-Quality Magnetotransport in Graphene Using the Edge-Free Corbino Geometry. *Phys. Rev. Lett.* **2019**, *122*, 137701.
(34) Schroeder, P. R.; Dresselhaus, M. S.; Javan, A. Location of Electron and Hole Carriers in Graphite from Laser Magnetoreflection Data. *Phys. Rev. Lett.* **1968**, *20*, 1292−1295.
(35) Toy, W. W.; Dresselhaus, M. S.; Dresselhaus, G. Minority Carriers in Graphite and the H-Point Magnetoreflection Spectra. *Phys. Rev. B* **1977**, *15*, 4077−4090.
(36) Doezema, R. E.; Datars, W. R.; Schaber, H.; van Schyndel, A. Far-Infrared Magnetospectroscopy of the Landau-Level Structure in Graphite. *Phys. Rev. B: Condens. Matter Mater. Phys.* **1979**, *19*, 4224−4230.
(37) Crassee, I.; Levallois, J.; van der Marel, D.; Walter, A. L.; Seyller, Th.; Kuzmenko, A. B. Multicomponent Magneto-Optical Conductivity of Multilayer Graphene on SiC. *Phys. Rev. B: Condens. Matter Mater. Phys.* **2011**, *84*, 035103.
(38) Booshehri, L. G.; Mielke, C. H.; Rickel, D. G.; Crooker, S. A.; Zhang, Q.; Ren, L.; Hároz, E. H.; Rustagi, A.; Stanton, C. J.; Jin, Z.; et al. Circular Polarization Dependent Cyclotron Resonance in Large-Area Graphene in Ultrahigh Magnetic Fields. *Phys. Rev. B: Condens. Matter Mater. Phys.* **2012**, *85*, 205407.
(39) Kharitonov, M. Phase Diagram for the $\nu = 0$ Quantum Hall State in Monolayer Graphene. *Phys. Rev. B: Condens. Matter Mater. Phys.* **2012**, *85*, 155439.

DOI: 10.1021/acs.nanolett.9b02505
Nano Lett. 2019, 19, 7043−7049

(40) Kunc, J.; Hu, Y.; Palmer, J.; Berger, C.; de Heer, W. A. A Method to Extract Pure Raman Spectrum of Epitaxial Graphene on SiC. *Appl. Phys. Lett.* **2013**, *103*, 201911.
(41) Jiang, Y.; Dun, Z. L.; Zhou, H. D.; Lu, Z.; Chen, K.-W.; Moon, S.; Besara, T.; Siegrist, T. M.; Baumbach, R. E.; Smirnov, D.; Jiang, Z. Landau-Level Spectroscopy of Massive Dirac Fermions in Single-Crystalline $ZrTe_5$ Thin Flakes. *Phys. Rev. B: Condens. Matter Mater. Phys.* **2017**, *96*, No. 041101(R).
(42) Orlita, M.; Faugeras, C.; Borysiuk, J.; Baranowski, J. M.; Strupiński, W.; Sprinkle, M.; Berger, C.; de Heer, W. A.; Basko, D. M.; Martinez, G.; Potemski, M. Magneto-Optics of Bilayer Inclusions in Multilayered Epitaxial Graphene on the Carbon Face of SiC. *Phys. Rev. B: Condens. Matter Mater. Phys.* **2011**, *83*, 125302.
(43) Faugeras, C.; Nerrière, A.; Potemski, M.; Mahmood, A.; Dujardin, E.; Berger, C.; de Heer, W. A. Few-Layer Graphene on SiC, Pyrolitic Graphite, and Graphene: A Raman Scattering Study. *Appl. Phys. Lett.* **2008**, *92*, 011914.
(44) Sprinkle, M.; Hicks, J.; Tejeda, A.; Taleb-Ibrahimi, A.; Le Fèvre, P.; Bertran, F.; Tinkey, H.; Clark, M. C.; Soukiassian, P.; Martinotti, D.; et al. Multilayer Epitaxial Graphene Grown on the SiC $(000\bar{1})$ Surface; Structure and Electronic Properties. *J. Phys. D: Appl. Phys.* **2010**, *43*, 374006.
(45) Siegel, D. A.; Hwang, C. G.; Fedorov, A. V.; Lanzara, A. Quasifreestanding Multilayer Graphene Films on the Carbon Face of SiC. *Phys. Rev. B: Condens. Matter Mater. Phys.* **2010**, *81*, 241417.
(46) Jiang, Z.; Henriksen, E. A.; Tung, L.-C.; Wang, Y.-J.; Schwartz, M. E.; Han, M. Y.; Kim, P.; Stormer, H. L. Infrared Spectroscopy of Landau Levels of Graphene. *Phys. Rev. Lett.* **2007**, *98*, 197403.
(47) Henriksen, E. A.; Jiang, Z.; Tung, L.-C.; Schwartz, M. E.; Takita, M.; Wang, Y.-J.; Kim, P.; Stormer, H. L. Cyclotron Resonance in Bilayer Graphene. *Phys. Rev. Lett.* **2008**, *100*, 087403.
(48) Deacon, R. S.; Chuang, K.-C.; Nicholas, R. J.; Novoselov, K. S.; Geim, A. K. Cyclotron Resonance Study of the Electron and Hole Velocity in Graphene Monolayers. *Phys. Rev. B: Condens. Matter Mater. Phys.* **2007**, *76*, No. 081406(R).
(49) Iyengar, A.; Wang, J.; Fertig, H. A.; Brey, L. Excitations from Filled Landau Levels in Graphene. *Phys. Rev. B: Condens. Matter Mater. Phys.* **2007**, *75*, 125430.
(50) Bychkov, Yu. A.; Martinez, G. Magnetoplasmon Excitations in Graphene for Filling Factors $\nu \leq 6$. *Phys. Rev. B: Condens. Matter Mater. Phys.* **2008**, *77*, 125417.
(51) Fuchs, J.-N.; Lederer, P. Spontaneous Parity Breaking of Graphene in the Quantum Hall Regime. *Phys. Rev. Lett.* **2007**, *98*, 016803.
(52) Li, Z. Q.; Henriksen, E. A.; Jiang, Z.; Hao, Z.; Martin, M. C.; Kim, P.; Stormer, H. L.; Basov, D. N. Dirac Charge Dynamics in Graphene by Infrared Spectroscopy. *Nat. Phys.* **2008**, *4*, 532−535.
(53) Poumirol, J. M.; Yu, W.; Chen, X.; Berger, C.; de Heer, W. A.; Smith, M. L.; Ohta, T.; Pan, W.; Goerbig, M. O.; Smirnov, D.; Jiang, Z. Magnetoplasmons in Quasineutral Epitaxial Graphene Nanoribbons. *Phys. Rev. Lett.* **2013**, *110*, 246803.
(54) Malard, L. M.; Nilsson, J.; Elias, D. C.; Brant, J. C.; Plentz, F.; Alves, E. S.; Castro Neto, A. H.; Pimenta, M. A. Probing the Electronic Structure of Bilayer Graphene by Raman Scattering. *Phys. Rev. B: Condens. Matter Mater. Phys.* **2007**, *76*, No. 201401(R).
(55) Zhang, L. M.; Li, Z. Q.; Basov, D. N.; Fogler, M. M.; Hao, Z.; Martin, M. C. Determination of the Electronic Structure of Bilayer Graphene from Infrared Spectroscopy. *Phys. Rev. B: Condens. Matter Mater. Phys.* **2008**, *78*, 235408.
(56) Li, Z. Q.; Henriksen, E. A.; Jiang, Z.; Hao, Z.; Martin, M. C.; Kim, P.; Stormer, H. L.; Basov, D. N. Band Structure Asymmetry of Bilayer Graphene Revealed by Infrared Spectroscopy. *Phys. Rev. Lett.* **2009**, *102*, 037403.
(57) Mak, K. F.; Lui, C. H.; Shan, J.; Heinz, T. F. Observation of an Electric-Field-Induced Band Gap in Bilayer Graphene by Infrared Spectroscopy. *Phys. Rev. Lett.* **2009**, *102*, 256405.
(58) McCann, E.; Koshino, M. The Electronic Properties of Bilayer Graphene. *Rep. Prog. Phys.* **2013**, *76*, 056503.
(59) Mucha-Kruczyński, M.; McCann, E.; Fal'ko, V. I. Electron-Hole Asymmetry and Energy Gaps in Bilayer Graphene. *Semicond. Sci. Technol.* **2010**, *25*, 033001.

DOI: 10.1021/acs.nanolett.9b02505
Nano Lett. 2019, 19, 7043−7049